A New Variant of Subgrid Dissipation for LES Method and Simulation of Laminar-Turbulent Transition in Subsonic Gas Flows

T.G. Elizarova[1], P.N. Nikolskii[2], and J.C. Lengrand[3]

[1] Institute for mathematical modeling RAS, Russia
[2] Dept. of Physics, Moscow State University, Russia
[3] CNRS/ICARE, France

Abstract

A novel variant of subgrid dissipation that may be used in LES methods is described and tested. The corresponding mathematical model, based on the quasi-gasdynamic equations differs from the Navier-Stokes system by additional nonlinear dissipative terms. This model is applied to the two-dimensional numerical simulation of the laminar-turbulent transition in a backward-facing step flow in subsonic regime.

1 Quasi-Gasdynamic Equations

The physical background for the quasi-gasdynamic (QGD) equations is based on a time-averaging technique involving a small control volume, taking into account a corresponding small time interval. This model generalizes the Navier-Stokes (NS) system of equations but differs from the NS system by additional dissipative terms which depend on a small multiplicative parameter τ (e.g. (Elizarova T.G., Sheretov Yu.V. 2001), (Elizarova T.G., 2005)). The QGD system may be written down in the form of conservation laws as

$$\frac{\partial \rho}{\partial t} + div\vec{j}_m = 0, \tag{1}$$

$$\frac{\partial (\rho\vec{u})}{\partial t} + div(\vec{j}_m \otimes \vec{u}) + \vec{\nabla} p = div\Pi, \tag{2}$$

$$\frac{\partial}{\partial t}\left[\rho\left(\frac{\vec{u}^2}{2}+\varepsilon\right)\right] + div\left[\vec{j}_m\left(\frac{\vec{u}^2}{2}+\varepsilon+\frac{p}{\rho}\right)\right] + div\vec{q} = div(\Pi\cdot\vec{u}), \tag{3}$$

with the closing relations

$$\vec{j}_m = \rho(\vec{u}-\vec{w}), \quad \text{where} \quad \vec{w} = \frac{\tau}{\rho}\left[div(\rho\vec{u}\otimes\vec{u}) + \vec{\nabla} p\right], \tag{4}$$

$$\Pi = \Pi_{NS} + \tau\vec{u}\otimes\left[\rho(\vec{u}\cdot\vec{\nabla})\vec{u} + \vec{\nabla} p\right] + \tau I\left[(\vec{u}\cdot\vec{\nabla})p + \gamma p div\vec{u}\right], \tag{5}$$

$$\vec{q} = \vec{q}_{NS} - \tau\rho\vec{u}\left[(\vec{u}\cdot\vec{\nabla})\varepsilon + p(\vec{u}\cdot\vec{\nabla})\left(\frac{1}{\rho}\right)\right]. \tag{6}$$

S.-H. Peng and W. Haase (Eds.): Adv. in Hybrid RANS-LES Modelling, NNFM 97, pp. 289–298, 2008.
springerlink.com

Here Π_{NS} and $\vec{q}_{NS}$ are the NS shear-stress tensor and the heat flux vector, respectively; τ is a small parameter with dimension of time. The system (1)–(6) is completed by the state equation for a perfect gas, and with expressions for the coefficients of viscosity, heat conductivity and parameter τ.

Heat conductivity coefficient κ and parameter τ are related through the viscosity coefficient μ by:

$$\kappa = \frac{\gamma \Re}{(\gamma - 1) Pr} \mu, \qquad \tau = \frac{\mu}{pSc}, \tag{7}$$

where Pr is the Prandtl number, Sc is the Schmidt number, $\Re$ is the perfect-gas constant, and γ is the specific heat ratio. For the viscosity thermal dependence we use the law $\mu = \mu_0 (T / T_0)^{\omega}$.

The QGD system differs from the NS one by second order space derivative terms of order $O(\tau)$. For stationary flows, the dissipative terms (terms in τ) in the QGD equations have the asymptotic order of $O(\tau^2)$ for $\tau \to 0$. For stationary Euler--flows, the terms in τ vanish. In the boundary layer limit, both QGD and NS equation systems reduce to Prandtl's system.

The entropy production X for the QGD system is the entropy production for the NS system completed by the additional terms in τ, that are squared left-hand sides of classical stationary Euler equations with positive coefficients:

$$X = \kappa \left(\frac{\vec{\nabla} T}{T} \right)^2 + \frac{(\Pi_{NS} : \Pi_{NS})}{2\mu T} + \frac{p\tau}{\rho^2 T} \left[div(\rho \vec{u}) \right]^2 + \\ + \frac{\tau}{\rho T} \left[\rho (\vec{u} \cdot \vec{\nabla}) \vec{u} + \vec{\nabla} p \right]^2 + \frac{\tau}{\rho \varepsilon T} [\rho (\vec{u} \cdot \vec{\nabla}) \varepsilon + p div \vec{u}]^2. \tag{8}$$

Equation (8) proves the dissipative nature of the additional τ-terms and the correctness of the QGD model with respect to the second law of thermodynamics.

In contrast to the NS system, continuity equation (1) of the QGD system is an equation of second order in space. Thus, the QGD system must be completed by an additional boundary condition. This condition for pressure p is obtained by imposing appropriate physical condition for the velocity $\vec{u}$ and for the mass flux vector $\vec{j}_m$ on a boundary. Investigations using the QGD system have been reported in (Elizarova T.G., Sheretov Yu.V. 2001), (Elizarova T.G., 2005) and citations therein.

Terms in τ allow constructing a family of novel numerical algorithms that inherit the mathematical properties of the QGD system. The QGD-algorithms are efficient in code implementation by virtue of the directly "built in" τ-regularization, ensuring a high quality of the numerical solution. The QGD-algorithms were successfully used in calculating a number of non-stationary gas dynamic problems, e.g. a flow around a body with a needle (Elizarova T.G., 1985), a flow in a hollow cylinder (Antonov A.N., 1990), and the Karman street flow (Elizarova T.G., 2007).

In this paper the QGD model is used as a new approach for numerical modeling of turbulent flows in the frameworks of the LES approximation. As a first example a two-dimensional numerical modeling of laminar-turbulent transition in the backward-facing step flow is presented. Additional subgrid dissipation is included in all gasdynamic equations in the form of strongly non-linear τ-terms.

2 Numerical Algorithm

A finite-difference approximation of the QGD system (1)–(6) is implemented using the control volume method. All gas dynamic parameters are determined at the nodes of the computational grid. The finite-difference approximations are attained in a flux form corresponding to conservation laws for the QGD equations, e.g. (Elizarova T.G., 2005), (Elizarova T.G., 2007).

An initial-boundary value problem is solved by applying a finite-difference scheme explicit in time. Spatial derivatives are approximated by central differences with second-order accuracy, while time derivatives are approximated by first order forward differences. The stability of the numerical algorithm is provided by the QGD terms in τ.

In the calculation of subsonic flows a term proportional to a grid step h is added to τ in the form

$$\tau = \frac{\mu}{pSc} + \alpha \frac{h}{c}, \tag{9}$$

where $c = \sqrt{\gamma \Re T}$ is the local sound velocity, and $0 \le \alpha \le 1$ is a numerical factor. The time step is chosen as $\Delta t = \beta h / c$ (Courant form), where the numerical coefficient $0 < \beta < 1$ is chosen according to the stability conditions along the computation.

3 Backward-Facing Step Flow Calculations

The test problem considered is a subsonic compressible viscous flow behind a backward-facing step, where the length of the separation zone strongly depends on Reynolds number, e.g. (Armaly B.F., 1983), (Wee D., 2004), (Rani H.P.,2006), (Langhe C.D., 2007) and works cited there.

We calculate the flow in a plane channel of length L and height $2H$ with a backward-facing step of height H, for $L=30H$. The flow is characterized by Reynolds and Mach numbers

$$\mathrm{Re} = \frac{\rho_0 U_0 H}{\mu_0}, \qquad Ma = \frac{U_0}{c_0}, \tag{10}$$

with density ρ_0 and temperature T_0 at inlet, where $U_0 = \int u_x dy$ is the mean entrance velocity.

Channel boundaries are supposed to be adiabatic with no-slip and non-penetrating velocity conditions. Poiseuille velocity profile and non-reflecting boundary conditions are imposed at the entrance and exit boundaries according to (Elizarova T.G., 2005), (Elizarova T.G., 2007). Gas flow with $u_x=u_y=0$, $\rho=\rho_0$, $T=T_0$ was taken as an initial condition.

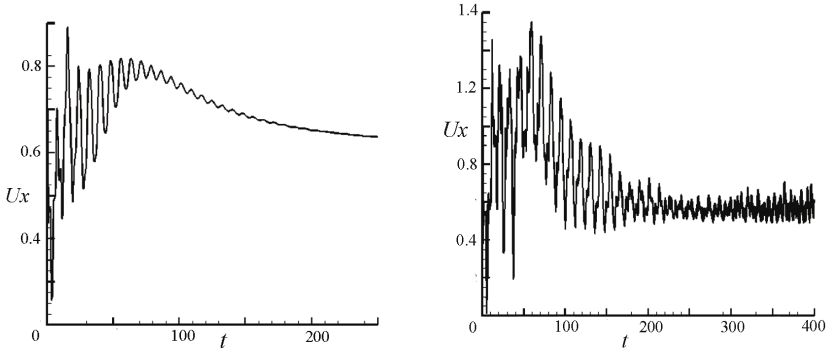

Fig. 1. Time-evolution of u_x for Re=300 (left) and Re=600 (right)

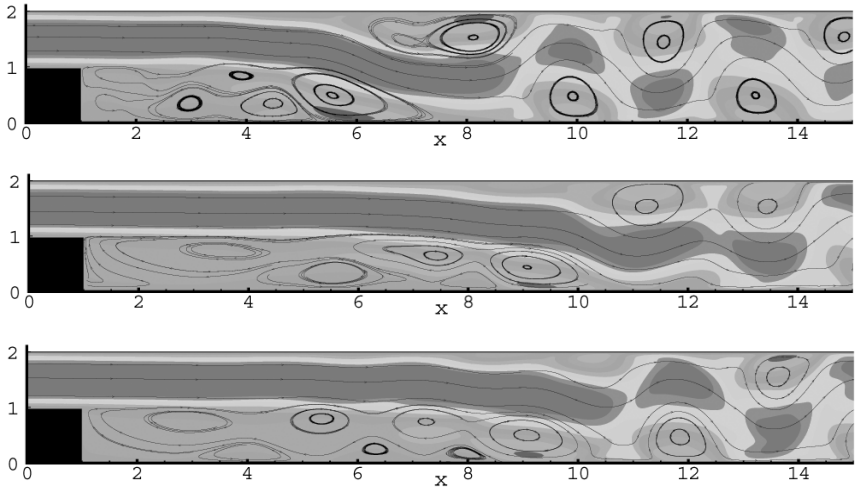

Fig. 2. Simultaneous stream functions and velocity iso-lines u_x for Re=1000, t=80, t=360, t=400, α=0.3, fragment

Several calculations were done for Reynolds numbers 100–3500 and Mach numbers 0.05–0.5 for air flow with γ=1.4, Pr=0.737, Sc=0.746, and ω=0.74, using uniform rectangular cells with h=0.1, 0.05, 0.03 and 2D computational domain. Small-scale motions in subgrid scale are described by τ-terms which are supposed to be isotropic, and large-scale motions are described in 2D formulation. The results for $Ma=0.1$ are presented below.

According to e.g. (Armaly B.F., 1983), the length of the separation zone L_s increases almost linearly for increasing Reynolds number, then reaches a maximum value, and finally it decreases. The increasing part is related with a laminar flow regime, and the decreasing part is related with the development of flow instabilities leading to a turbulent regime.

For small Reynolds numbers (laminar regime) the numerical calculations lead to a stationary flow, and the results are in a good agreement with the NS numerical modeling and with experiment. Here terms in τ do not affect the NS solution and act as a numerical regularizator. The time evolution of the velocity at Re=300 and 600 are shown in fig.1. The onset of non-stationary flow is shown for Re=600. These results correspond to h=0.05, α=0.5 and β=0.3.

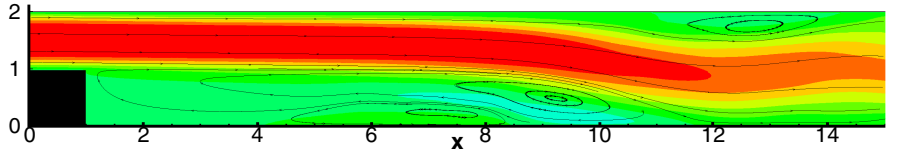

Fig. 3. Stream function and velocity isolines u_x for time-averaged flow, Re=1000, fragment

For increasing values of Re the flow becomes strongly non-stationary and the length of the separation zone must be found by time-averaging. Here the terms in τ become important and act as a subgrid turbulent dissipation. Fig.2 shows a set of instantaneous flow pictures for Re =1000, h=0.03, α=0.3 and β=0.5. In fig.3 a corresponding time-average picture is presented. Fig.4 shows an averaged flow for Re=3500. 3D computations are made by V.V. Seregin for h=0.1, α=0.5. Compared with the laminar flows, the inner structure of a time-averaged separated flow in the turbulent regime includes additional near-wall vortices (figs.3, 4).

The flow pictures shown in figs.2—4 qualitatively agree with the results (Wee D., 2004) obtained in 2D computations for Re=3700 by a developed variation of the random vortex method together with a finite element approximation.

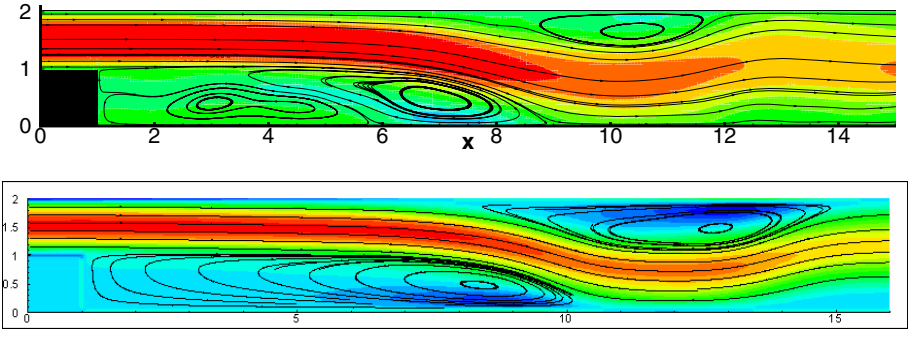

Fig. 4. Stream function and velocity iso-lines ux for time-averaged flow, Re=3500, Fragments. Upper fig.- 2D calculation, lower fig. – 3D calculations.

Fig.5 shows an example of a temporal evolution of the velocity at *Re*=1000 and 3500. Fig.6 shows the skin-friction coefficient behind a step, calculated for a time-averaged flow at *Re*=3500. Qualitatively it agrees with the results obtained in (Langhe C.D., 2007) by RANS/LES and DNS simulations at *Re*=5100.

In Fig.7 calculated values of the length L_s (normalized in H) of the recirculation zone behind a step are compared with the experimental values from (Armaly B.F., 1983, where *Re* was based on a length ~2*H*). It shows a reasonable agreement between computation and experiment both for laminar regimes and for non-developed turbulent regimes, including the point of bifurcation. The non-monotonous behavior of L_s for $Re > 1000$ could be related with the onset of three-dimensional structures in the flow that cannot be simulated in the present 2D modeling. The point of bifurcation obtained in these QGD 2D calculations approximately corresponds to experimental results from (Armaly B.F., 1983) and to the bifurcation point at *Re*=738 from the bifurcation diagram of (Rani H.P., 2006).

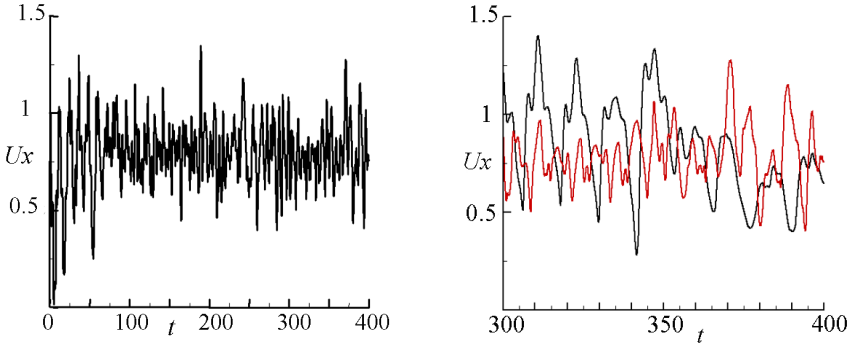

Fig. 5. Temporal velocity evolutions at *Re*=3500 (left) and a fragment of velocity-evolution in two space points at *Re*=1000 (right)

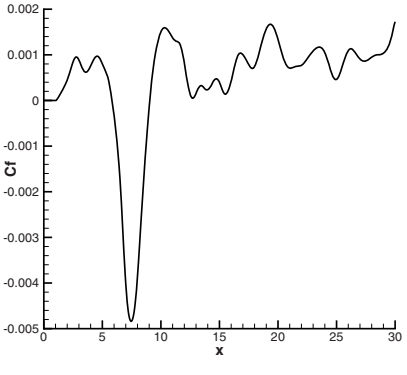

Fig. 6. Skin-friction coefficient behind a backward-facing step at *Re*=3500

A unified numerical method with only one free parameter is used for both laminar and turbulent regimes. This free parameter is the coefficient α in (9), where h/c corresponds to a time for sound-velocity disturbances to cross a computational cell. The calculations for laminar flows show that factor α acts only on the stability of the QGD algorithm: with $\alpha \to 0$, the numerical time step must tend to zero ($\Delta t \to 0$) to ensure stability. However the solution does not depend on α. On the contrary, for strongly non-stationary turbulent flows, the numerical solution depends on α. The lengths L_s of the separation zones calculated for α = 0.5 and 0.3 are shown in fig.7. Both solutions are mutually consistent and are consistent with experiment for laminar flows with Re<600. The solutions also agrees with experiment for turbulent flows with Re>600. The dependence of the solution on α-coefficient for turbulent flows must be studied using finer space steps h and 3D computational grids, providing increased resolution of vortex structures and energy spectrum.

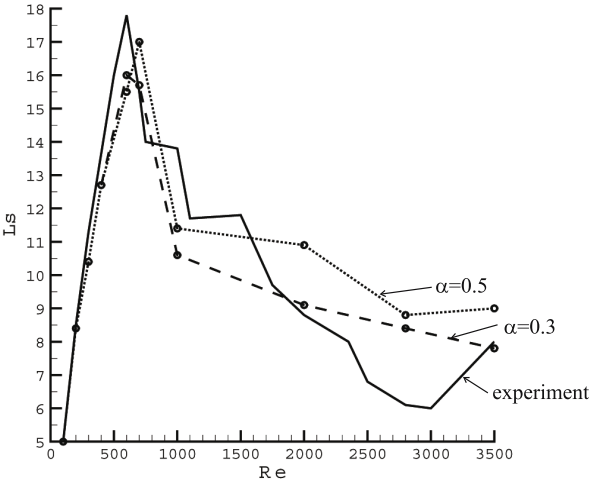

Fig. 7. Separation zone length. Dash-lines - calculations, full line – experimental data (Armaly B.F., 1983)

A set of 2D computations has been performed under conditions corresponding to experiments carried out in LME (France, Orleans) using a wind tunnel adapted for low velocities. Particle Image Velocimetry (PIV) was used to measure the mean velocity field in a symmetry plane. Here, in contrast with the previous cases, the initial velocity profile is supposed to be uniform. Experiments and computational results in the framework of the QGD-family model for incompressible flows have been reported in (Elizarova T.G., Shilnikov E.V., Weber R., 2004).

In Fig.8 experimental flow fields obtained by averaging over three different time intervals (Δt ~10 -- 50 in non-dimensional values) are shown together with a computational time-average flow field for $Ma=0.1$. A two-vortex structure in the computational and experimental patterns is clearly seen. The position of the main vortex is well predicted by computation. In fig.9 the flow fields are obtained by

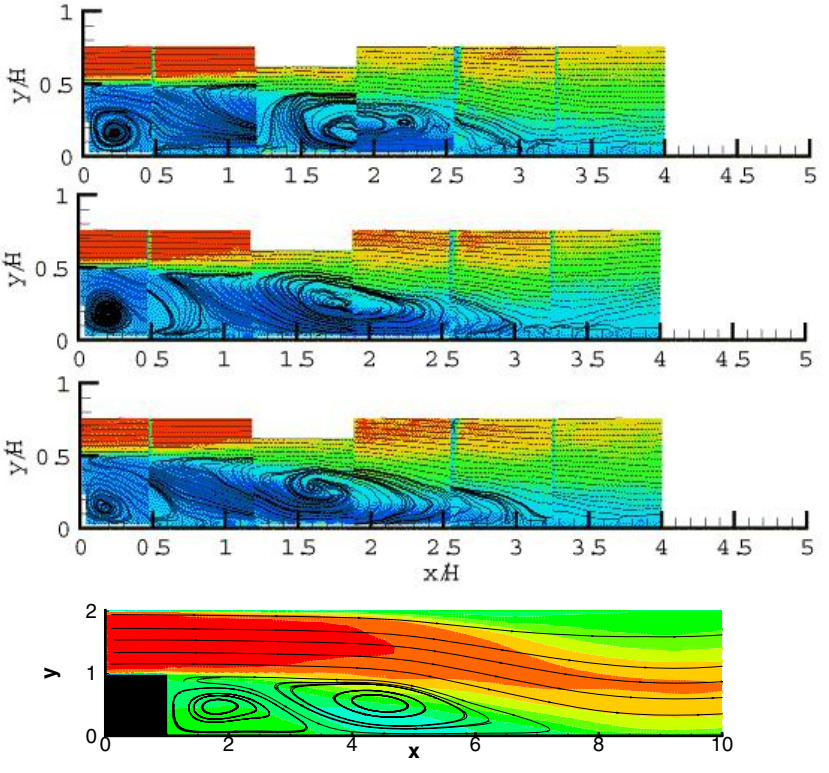

Fig. 8. Averaged flow field, *Re*=4667, experimental pictures from (Elizarova T.G., Weber R., 2004) (upper figs.) and calculations (lower fig.)

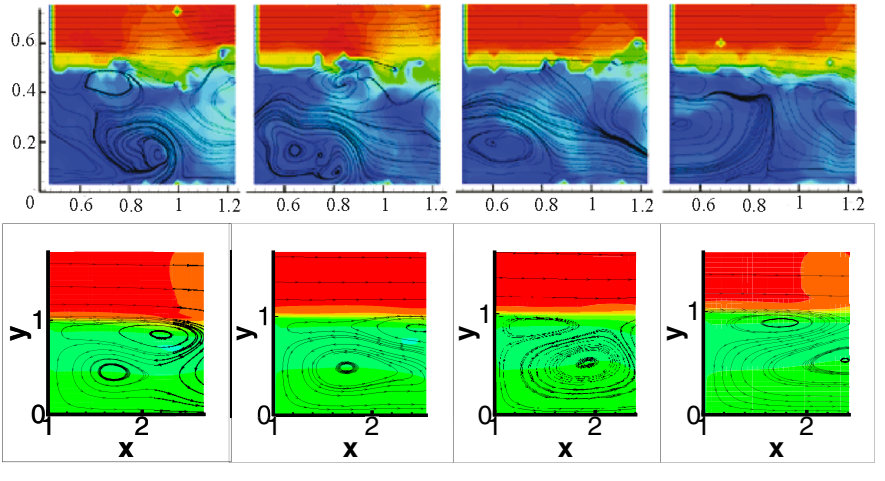

Fig. 9. Fragments of an averaged flow field, small time interval, *Re*=4667, experimental data from (Elizarova T.G., Weber R., 2004) (upper figs.) and calculations (lower figs)

averaging the corresponding instantaneous velocity patterns over a small time interval (Δt ~0.1 in non-dimensional values). For both time-averaging intervals the calculated and the measured flow structures have the same character.

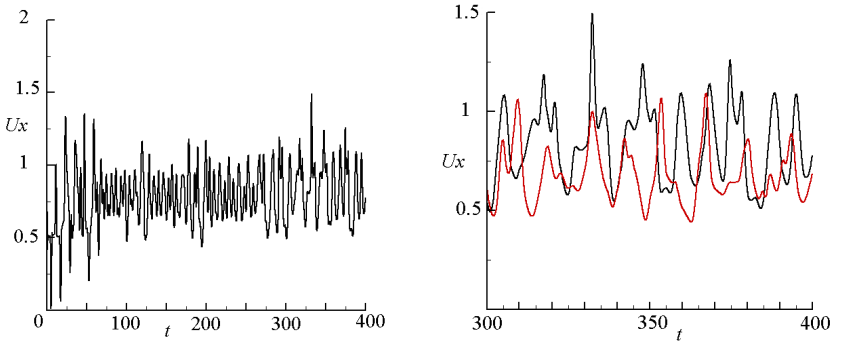

Fig. 10. Temporal velocity evolutions for *Re*=4667 (left) and it fragment of velocity evolution in two space points (right)

The main Strouhal-frequency obtained in numerical computations at *Re*=4667 is $Sh=fH/U_0$~0.08, where *f* is the main frequency (fig.10). This result is comparable with DNS and RANS/LES flow pictures reported in (Langhe C.D., 2007) for 3D test flow with the Strouhal-frequency 0.066<*Sh*<0.08 for *Re*=5100, and also with *Sh*~0.07 for *Re*=3700 (Wee D., 2004) in 2D calculations.

Fig.11 shows energy spectra *E(k)* in linear (left) and logarithm (right) scales for *Re*=1000, 3500 and 4667. The Kolmogorov-Oboukhov's energy dissipation law in spectral form $E(k) \sim k^{-5/3}$ is shown for comparison. This law is valid for developed turbulent regimes and qualitatively is not contradictory with the present computations.

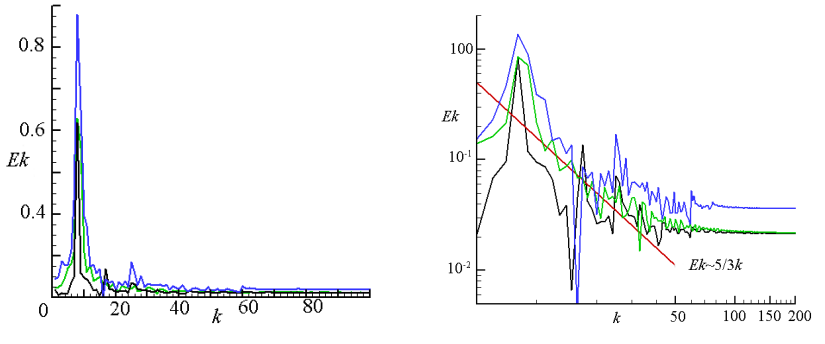

Fig. 11. Energy spectra for Re=1000, 3500 and 4667 together with Kolmogorov-Oboukhov energy dissipation law

4 Conclusions

The present computations on a backward-facing step flow show that the QGD model provides a numerical simulation for both laminar and turbulent flows, including the transition between these regimes. Even in 2D formulation the present model allows to simulate the main features of the flow. The simple structure of the present algorithm is well suited for 3D numerical computations, which implies parallel computing.

The QGD model employs a unified computational algorithm with only one free parameter. The advantages of the model in laminar and turbulent flow modeling follow from the validity of basic fluid dynamic conservation laws, well established for the QGD equation system.

The QGD dissipation can be used as a novel variant of subgrid dissipation in LES methods.

References

Antonov, A.N., et al.: Numerical simulation of pulsating regims in supersonic flow around a hollow cylinder. Comp. Math. and Math. Phys. 30, 548 (1990)

Armaly, B.F., et al.: Experimental and theoretical investigation of backward-facing step flow. J. of Fluid Mech. 127, 473–496 (1983)

Elizarova, T.G., Khokhlov, A.A., Sheretov Yu, V.: Quasi-gasdynamic numerical algorithm for gas flow simulations. In: ICFD 2007, University of Reading, UK (2007)

Elizarova, T.G., Pavlov, A.N., Chetverushkin, B.N.: Using kinetical algorithm for calculation gasdynamical flows. J. diff. equations 21(7), 1180–1185 (1985)

Elizarova, T.G., Sheretov Yu, V.: Theoretical and numerical analysis of quasi-gasdynamic and quasi-hydrodynamic equations. Comp. Math. and Math. Phys. 41, 219 (2001)

Elizarova, T.G., Sheretov Yu, V., Sokolova, M.E.: Quasi-gasdynamic equations and numerical simulation of viscous gas flows. Comp. Math. and Math. Phys. 45, 545 (2005)

Elizarova, T.G., et al.: Separated flow behind a backward-facing step. Part II. Experimental and numerical investigation of a turbulent flow (2004), http://arXiv.org/abs/math-ph/0410023

Elizarova, T.G., et al.: Experimental and numerical investigation of the turbulent flow behind a backward-facing step. In: BAIL conference, France, Toulouse (2004)

Langhe, C.D., Merci, B., Dick, E.: Renormalization group based hybrid RANS/LES modeling. ERCOFTAG bulletin 72, 55–59 (2007)

Rani, H.P., Sheu, T.W.H.: Nonlinear dynamics in a backward-facing step flow. Physics of Fluids 18, 84101 (2006)

Wee, D., Tongxun, Y., Annaswamy, A., et al.: Self-sustained oscillations and vortex shedding in backward–facing step flows: Simulation and linear instability analysis. Physics of Fluids 16(9), 3361–3373 (2004)